Global Biogeochemical Cycles

Supporting Information for

Ironing Out Fe Residence Time in the Dynamic Upper Ocean

E. E. Black[1,2,3], S. S. Kienast[2], N. Lemaitre[4], P. J. Lam[5], R. F. Anderson[3], H. Planquette[6], F. Planchon[6], and K. O. Buesseler[1]

[1]Department of Marine Chemistry & Geochemistry, Woods Hole Oceanographic Institution, 266 Woods Hole Road, MS25, Woods Hole, MA, 02543, USA.

[2]Department of Oceanography, Dalhousie University, 1355 Oxford St, PO Box 15000, Halifax, NS, B3H 4R2, Canada.

[3]Division of Geochemistry, Lamont Doherty Earth Observatory, 61 Route 9W, PO Box 1000, Palisades, NY, 10964, USA.

[4]Department of Earth Sciences, Institute of Geochemistry and Petrology, ETH-Zürich, Clausiusstrasse 25, 8092 Zürich, Switzerland.

[5]Department of Ocean Sciences, University of California, Santa Cruz, CA, 95064 USA.

[6]Univ Brest, CNRS, IRD, Ifremer, LEMAR, F-29280 Plouzané, France.

Contents of this file

Table S5: Testing different approaches for the use of below detection limit results from the Pacific (cruise TN303) with iron export flux calculations
Table S6: Testing different approaches for the use of below detection limit results from the Pacific (cruise TN303) with iron inventory calculations

Additional Supporting Information (Files uploaded separately)

Captions for Tables S1 to S2 (metadata included with the .xlsx file)

Table S1: Study information and results related to iron export (flux) measurements. (included in separate file 'Blacketal_TablesS1_S2.xlsx)

Table S2: Study information and results related to iron residence time estimates. (included in separate file 'Blacketal_TablesS1_S2.xlsx)

Introduction

S1 includes a more in-depth look at the drivers of global Fe export, one of the parameters defining Fe residence time. This supplement expands on the statistics described in the main text Section 3.1 and Table S3. The instances where we find no correlation are particularly informative.

S2 provides a detailed explanation of all methods and the means of data evaluation.

Figures S1 to S5 provide graphical support for minor points made in the main text and help summarize aspects of our data compilation. For example, Figure S1 condenses the data pattern observed in Figure 2, Figure 4, and Table 2 into a purely pictorial form. Figure S4 quickly illustrates to the reader the reason for deeming certain points anomalous and how the main text Figure 2 looks when separated by methodology.

Tables S1 and S2 contain the derived parameters and results unique to this study, as well as all the prior estimates of Fe export from ^{234}Th and sediment trap studies. As such, theses tables are too large to be included in a word file and are provided in a format that can be easily used in computing environments, such as matlab (e.g. absent values = NaN). Table S3 provides additional statistical results that reflect all the tested regressions, not just those presented in the main text. Table S4 contains the ^{234}Th fluxes used in this study for the TN303, KN204-01, and KN199-04 cruises. These are parameters that can be derived from the publicly available ^{234}Th data (see Data Availability), but for ease of use, we report them here. Tables S5 and S6 illustrate how below detection limit Fe data was utilized, according to the methodology outlined in S3.

SUPPLEMENTAL TEXTS

Text S1. On the drivers of global Fe export.

One of the chief findings of this study is that most estimates of the residence time of total Fe (τ_{tot}) fall in a narrow, 10- to 100-day range. To further evaluate the factors potentially influencing this range, we can look at what impacts the parameters that define it: the export flux of Fe (y-axis, Fig. 3a) and inventory of Fe (x-axis, Fig. 3a). The export flux of Fe from the surface and the remaining inventory are the result of a dynamic battle between export stimulating processes and processes that favor Fe retention or recycling. The result of these dueling factors, including aggregation-disaggregation, grazing-egestion, uptake-remineralization, and solubilization-scavenging, is varying amounts of Fe being incorporated in sinking material in different regions of the global ocean. While differentiating the relative importance of each process is difficult, especially by region, we can assess potential proxies for Fe 'packaging' in particulate matter, such as carbon export or productivity.

Most measurements of Fe export prior to the late 2000s came from moored sediment traps or drifting traps at time-series sites (e.g. BATS and HOT, Table 1). The international GEOTRACES program now has added a plethora of total iron export (F_{tot}) along basin-scale transects and in island-proximal Southern Ocean regions using ^{234}Th rather than traps (Table 1; Figure 1). The large variability in F_{tot} observed within a region (Quetel et al., 1993), over a season or year (Collier et al., 2000), and between methods (Bowie et al., 2015; Lemaitre et al., 2016) (Figure S4) makes a quantitative assessment of global controls on F_{tot} challenging. Within coastal shelf and slope regions, 10-fold variations in F_{tot} have been observed and local factors, such as currents and shelf width could play an important role over these smaller spatial scales (Smith et al., 2014). Furthermore, our best model-based estimate for dust supply, a factor thought to play a large role in setting F_{tot}, shows no relationship to *in-situ* estimates of F_{tot} or total Fe inventories ($r^2 < 0.1$, Figure S2-C and Figure S2-E; Table S3). The relationship between modeled dust supply and dissolved Fe inventories is only slightly better ($r^2 = 0.23$, Table S3). This likely results from a methodological mismatch, e.g. the sporadic nature of dust events at one location is not well represented by outputs from current global models, the inability of dust models to accurately reproduce local-regional conditions (e.g. Winckler et al., 2008), and the influence of multiple sources and processes on Fe cycling. However, when distance-to-coast is used as a proxy for dust inputs and supply from margin sediments, we see a stronger, inverse relationship with F_{tot} ($r^2 = 0.46$, Figure S2-G and Figure S3-A) and total Fe inventory ($r^2 = 0.40$, Figure S2-I). These results suggest that distance-to-coast is a more comprehensive source proxy for Fe at the basin-scale than either dust inputs or the supply of dissolved Fe from sediments by themselves. This is relevant because the regional flux of dissolved Fe from sediments to the water column is often poorly known (Homoky et al., 2016) and local measurements can vary from 10 to >800 μmol Fe m^{-2} d^{-1} in areas like the Peruvian margin (Noffke et al., 2012). As such, sites are grouped in this study by distance-to-coast (or to major island chain) along with latitude and biogeochemical Longhurst Provinces (Longhurst, 2007).

Annual Chl-a, an indicator of phytoplankton biomass, shows a positive relationship with total Fe inventories (r^2 = 0.33) and F_{tot} (r^2 = 0.42, Table S3). Simultaneous measures of the export of particulate organic carbon (F_{POC}) also show a positive relationship with F_{tot} (r^2 = 0.40, Figure S3-A and Figure S3-B) and to a lesser extent with Fe inventories ($r^2 \leq$ 0.14, Table S3). At the basin scale, annual Chl-a and F_{POC} likely best reflect the biological processes that package Fe in exportable particles and in part, set the magnitude of F_{tot}. In short, high Fe supply is balanced by high Fe export and can stimulate high Chl-a and F_{POC}. When distance-to-coast, F_{POC}, and F_{tot} are combined, the resulting multiple linear regression explains more than half of the variability in F_{tot} (r^2 = 0.52, Table S3). The regression for distance-to-coast, annual Chl-a, and F_{tot} is comparable (r^2 = 0.48, Table S3), suggesting that productivity and the processes that contribute to F_{POC} both have a robust link to F_{tot}.

We also note that net primary productivity (NPP) for the 16 days prior to sampling did not show a correlation with Fe inventories or F_{tot} ($r^2 \leq$ 0.01, Table S3). A lack of correlation might result from the number of processing steps between the initial ocean color image and the final NPP estimate or could indicate that the biological factors impacting iron cycling might not be accurately reflected in a 16-day prior average. It is curious though that the r^2 between annual Chl-a and Fe inventories are so much better than that of the 16-day NPP. Perhaps annual Chl-a more accurately reflects the long-term rate of Fe supply (proportional to total Fe inventory) in regions where the residence time of total Fe is highly variable in time.

F_{POC} and F_{tot} are strongly correlated (r^2 = 0.57) in the high-nutrient low-chlorophyll (HNLC) Subantarctic and high-latitude North Atlantic (HLNA) regions (Figure S3-C), suggesting that F_{tot} and F_{POC} are more tightly coupled in these areas of the ocean. Furthermore, the same magnitude of F_{tot} (y-axis, Figure S3-B and Figure S3-C) is associated with a higher magnitude of F_{POC} (x-axis) in an HNLC or HLNA (black and grey) when compared to the other regions (pink, white, and blue), as indicated by the steeper regression. For the Southern Ocean, a known HNLC region, this observation could be consistent with paleoceanographic evidence of elevated export production and nitrate utilization at times of high Fe flux to the sediments during cold intervals of the last glacial cycle (Martínez-García et al., 2014). Whereas the greater nitrate utilization during cold intervals is logically the results of Fe fertilization, the enhanced export production during cold intervals resulted from the synergistic effects of greater macronutrient supply coincident with periods of greater dust flux (Anderson et al., 2014).

Text S2. Methods.

2.1 Evaluation and use of ^{234}Th flux data from TN303, KN199-04, and KN204-01

All the 100 m and 200 m ^{234}Th fluxes from TN303 ('Pacific') and KN199-04 and KN204-01 ('Atlantic') are reported in Table S4. For the Pacific campaign, ^{234}Th fluxes were measurable at all stations where particulate samples were collected except at the two

easternmost stations, where the determination of the flux of ^{234}Th at 200 m was not possible (bottom depth<200 m). ^{234}Th fluxes were smaller in the Atlantic, on average. There were six instances (two at 100 m and four at 200 m) in the Atlantic where the uncertainty on the flux estimate was greater than the flux determined. In this case, the large uncertainty results from a propagated uncertainty on the small difference between two large numbers, the total ^{234}Th inventory and total ^{238}U inventory, when inventories are summed into the cumulative flux of ^{234}Th at a given depth. The uncertainty on the cumulative flux of ^{234}Th increases with depth due to the error propagation, despite similar uncertainties on each individual total ^{234}Th measurements. We have calculated the Fe flux at these 'low flux' locations (note [a], Table S4) to provide a gauge for the lower bounds on Fe fluxes in these regions, but these data should not be used elsewhere. There were also three instances in the Atlantic where the flux estimates were negative. In these cases, we did not determine any Fe fluxes or residence times at these locations and the ^{234}Th data have not been reported. In summary, a total of 41 stations had useable ^{234}Th data for Fe flux calculations at 100 m and 34 stations had useable data at 200 m.

2.2 Evaluation and use of iron concentration data from TN303, KN199-04, and KN204-01

None of the large (LP) or small (SP) particle Fe concentration data from the Atlantic had been flagged as 'questionable' or of 'bad' quality and all were used in calculating Fe:^{234}Th (for Fe flux determination) and Fe inventories. For the Pacific dataset, the particulate concentration detection limits were defined as three times the standard deviation of the dipped filter blanks and any positive measurement results below these limits were flagged as 'questionable'. In the upper 200 m, 43 of the 89 large particle concentration results were below the detection limit of 0.02 nM (BDL), although 74% of the results were within 1 s.d. of the detection limit. The abundance of 'low' results in the Pacific is unsurprising considering the 0 to 200 m range in large particle Fe concentrations of 0.001 nM to 13 nM (mean 0.6 nM) for this cruise compared to the 0.04 nM to 26 nM range (mean 1.1 nM) observed for the Atlantic cruise. The detection limit for the small particle concentrations was an order of magnitude higher at 0.14 nM, which resulted in 41 of 89 small particle concentration measurements being flagged in the same manner for the Pacific cruise, but only 5% of these were within 1 s.d. of the detection limit.

The impact of the utilization of the $[Fe]_{LP}$ BDL data on Fe export results was tested for three cases: (1) All $[Fe]_{LP}$ BDL were used as measured, (2) all BDL $[Fe]_{LP}$ were set to the detection limit, and (3) all BDL $[Fe]_{LP}$ were removed before flux calculations (Table S5). Completely removing the Pacific BDL $[Fe]_{LP}$ results from the Fe:^{234}Th (flux) calculations either led to an overestimation of the fluxes at and around the depths of the BDL results or led to no result due to a lack of data (Case 3, Table S5). For instance, if the original $[Fe]_{LP}$ measurements were made at 50 m (1 nM), 75 m (0.01 nM), and 100 m (0.05 nM), the absence of the 75 m measurement would mean that the 50 m and 100 m are used to interpolate the $[Fe]_{LP}$ at all the depths in between, including 75 m. In this case, the interpolated $[Fe]_{LP}$ derived from data at 50 m and at 100 m would all be above 0.05 nM.

To better represent the occurrence and magnitude of these BDL results, we have set the Pacific large and small particle concentrations that were flagged as BDL to the respective detection limits (Case 2). This change increases the Fe fluxes slightly because the reported results were below this limit. However, as shown in Table S5, the zonal averages of the flux at 100 m are almost identical whether the BDL $[Fe]_{LP}$ results are used as is or set to the detection limit. The reported fluxes in this study all use the Case 2 method and can be thought of as 'maximum possible' fluxes, although the comparison of the methods suggests this designation is not necessary.

The inventory estimates, on the other hand, differed depending on which use of the [Fe] BDL results was applied (Table S6) and illustrate the consequences of data removal. The large particle inventory estimates not utilizing the BDL $[Fe]_{LP}$ results and the total inventory estimates not utilizing the $[Fe]_{LP}$ BDL and $[Fe]_{SP}$ BDL results showed the greatest differences from the other two methods and the pattern of difference was inconsistent (e.g., Case 3, where all BDL values were removed, had higher Pacific station 9 inventories and lower Pacific station 32 inventories than for Cases 1, where BDL values were used as measured, or Case 2, where values were set to the detection limit). While the Case 1 and Case 2 inventory estimates are close, Case 2 (the method used in this study) always had higher results. Therefore, all inventories reported in this study should be considered 'maximum possible', as should the derived residence times, equal to inventory divided by flux, because the inventories were impacted more substantially than the fluxes (Table S5 and Table S6).

For both the Pacific and Atlantic, all the dissolved Fe concentration data used from the upper 800 m was flagged as 'good' and no data adjustments had to be made.

2.3 Collection and processing of particulate samples for GEOVIDE campaign

Methods used to collect and process samples on the GEOVIDE (North Atlantic GA01) section have been described in N. Lemaitre's Ph.D. thesis (Lemaitre, 2017) and follow the recommendations contained in the GEOTRACES Cookbook http://geotraces.org/images/stories/documents/intercalibration/Cookbook.pdf, but have not been published previously. Particles were collected using *in-situ* large volume filtration systems (ISP hereafter) through paired 142 mm-diameter filters: a 53 µm mesh nylon screen (Petex; polyester) and a 0.8 µm polyestersulfone filter (Supor). Before use, filters were placed in an acid cleaned containers containing 1.2M HCl (Suprapur grade, Merck). The containers were then double bagged in Ziploc bags and placed in an oven at 60°C overnight. After cooling, the acid solution was removed and filters were thoroughly rinsed with Milli-Q water. Due to the slow release of acid from the filters, this rinsing step took days in order to reach a pH value slightly less than 7. Filters were then kept in the LDPE bottles filled with Milli-Q until use.

On board, filters were processed under a laminar flow unit within a customized clean "bubble" to prevent any contamination issues. Before and after the ISP recoveries, pump

heads were also covered with plastic bags to minimize contamination. After pump recoveries, filter heads were dismantled and carried inside the clean bubble. Under the laminar flow hood, the 142 mm filters were then subsampled as follows: using a clean ceramic scalpel, one quarter of the PETEX, dedicated to ^{234}Th analyses in the large size fraction (LSF; >53 µm), was cut out. Then, particles were washed off this PETEX quarter using 0.45 µm filtered seawater (collected during the GEOVIDE cruise) through polyethersulfone filters (Supor®, porosity = 0.45 µm, diameter = 25 mm) mounted on a polysulfone filtration unit (Pall). Supor filters were then dried under the laminar flow unit and mounted on nylon holders, covered with Mylar and aluminum foil for analysis by Beta counting (low level beta counters, RISØ, Denmark). A second quarter of the PETEX which was dedicated to trace element analyses in the LSF was kept in a clean Petri slide (Millipore) at -20°C until sample processing and subsequent analysis in the home laboratory. The two remaining PETEX quarters were stored in clean Petri slides (Millipore) at -20°C for further analyses carried by other teams. The seawater volume filtered through a PETEX quarter was typically between 23 and 370 L. The 142 mm Supor filter was also subsampled for TE, major element and BSi analyses in the small size fraction (SSF; 1-53 µm), using a 13 mm diameter disposable skin biopsy Acupunch. The seawater volume filtered through these punches was typically between 1 and 13 L. These punches were not Beta counted to avoid potential contamination of the samples and were directly stored in clean Petri slides double bagged in Ziploc bags and stored at -20°C until analysis.

Particles on the nylon screen were washed off the filter with 0.45 µm filtered surface seawater (sampled during the cruise at Station 77, 40m) and collected on acid cleaned 47 mm diameter mixed cellulose esters filters (MF-Millipore® filters, 0.8 µm), mounted on acid cleaned polysulfone filtration units (Nalgene®). This seawater has a dissolved iron (dFe) concentration of 0.102 ± 0.019 nmol L^{-1}. The MF filter was then cut in two equal parts using an acid clean ceramic scalpel in order to digest totally the first half and to leach the second half (see below).

Under a Class-100 clean fume hood, one 13 mm punch of the Supor filter (SSF) or a half of the 47 mm MF filter (LSF) was placed along the wall of a 15 mL acid cleaned Teflon vial (Savillex). Then, 2 mL of a solution 8M HNO_3 (Ultrapur grade, Merck) and 2.3M HF (Suprapur grade, Merck) was added. Vials were then refluxed at 130°C on a hotplate during 4h. After gentle evaporation close to near dryness, 200 µL of concentrated HNO_3 (Ultrapur grade, Merck) was added in order to drive off the fluorides. The residue was brought back into solution with 3% HNO3 spiked with 1 µg L^{-1} of Indium and stored in acid cleaned 15 mL centrifuge tubes (Corning) until analysis for estimating the total particulate trace elements concentrations.

All measurements for trace elements were performed using a SF-ICP-MS (Element 2, Thermo) following the method of Planquette and Sherrell (Planquette & Sherrell, 2012). Sample introduction system consisted of a FAST valve, a PFA nebulizer and a double stage spray chamber. Every 11 samples, a replicate analysis of a selected sample digest

solution was made. The precision and the accuracy of our analyses were assessed by measuring replicates and the Certified Reference Materials (CRM) BCR-414, respectively. External calibration curves were run at the beginning, middle and end of the run. Since then, other CRMs (sedimentary materials PACS-3 and MESS-4) have been digested using the same analytical method and good recoveries were achieved.

SUPPLEMENTAL FIGURES

Figure S1. Global patterns observed in upper ocean Fe inventory, Fe export, and total Fe residence time. Box size indicates relative Fe inventory and outline colors match the zones indicated in Figure 1. The vertical arrows reflect the relative amounts of F_{lith} (black) , F_{auth}, (gray) and F_{bio} (green) within F_{tot} (y-axis) that were observed in each region. The relative magnitude of F_{POC} is indicated by the colorbar shown to the right (~1 to 10 µmol m^{-2} d^{-1}), with deeper greens reflecting larger F_{POC}. Inset: arrows indicate how changes in Fe sources and surface processes influence total Fe inventory and F_{tot} to keep the total upper ocean residence time of iron in the narrow 10- to 100-day range. Export stimulating processes include both biotic and abiotic processes, such as scavenging and aggregation. Retention and recycling refer to processes that retain Fe in the upper ocean, such as remineralization and complexation.

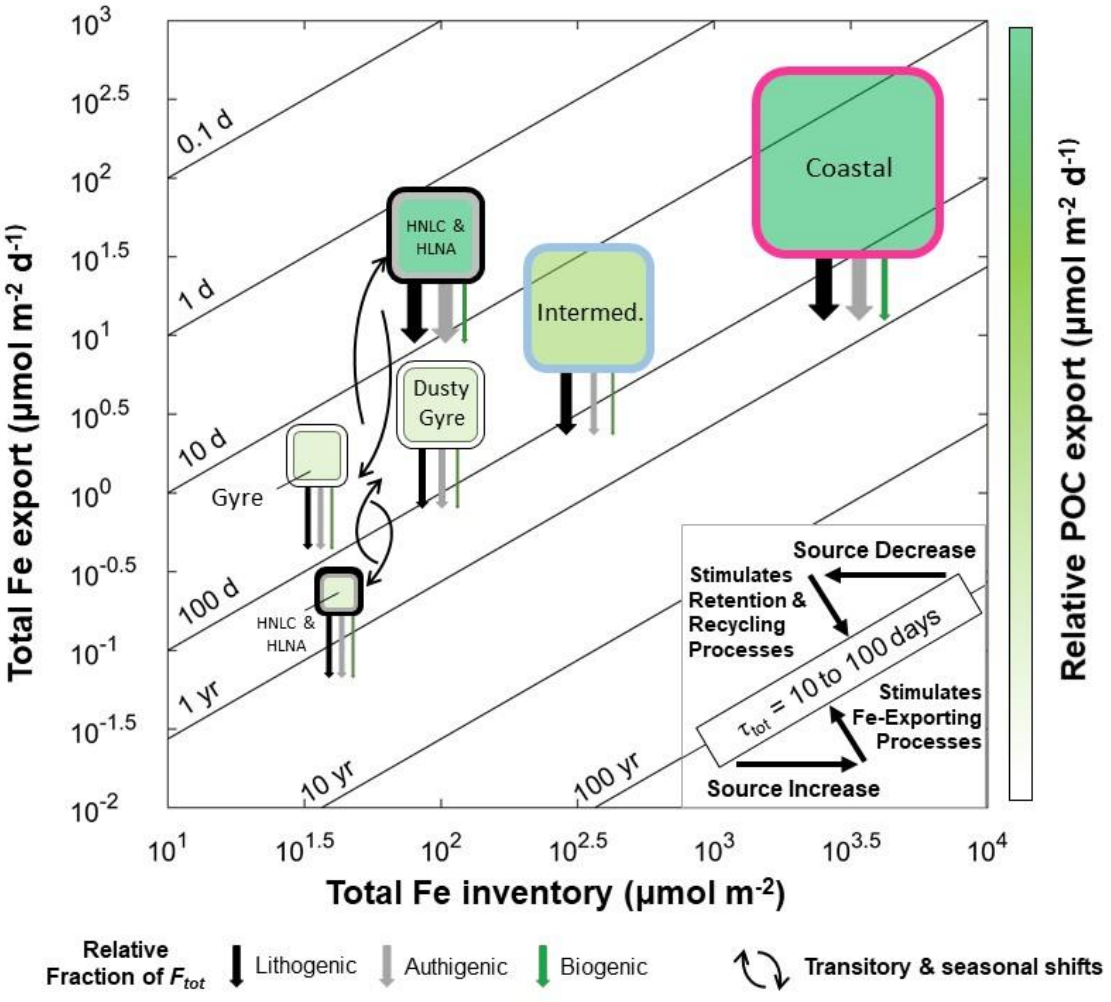

Figure S2. Regression and residual results. Panels A, C, E, G, and I are log-log plots of data from locations where F_{tot}, total Fe inventories, and the input fluxes of Fe from dust (modeled) were available. The fits are linear regressions with the 95% confidence

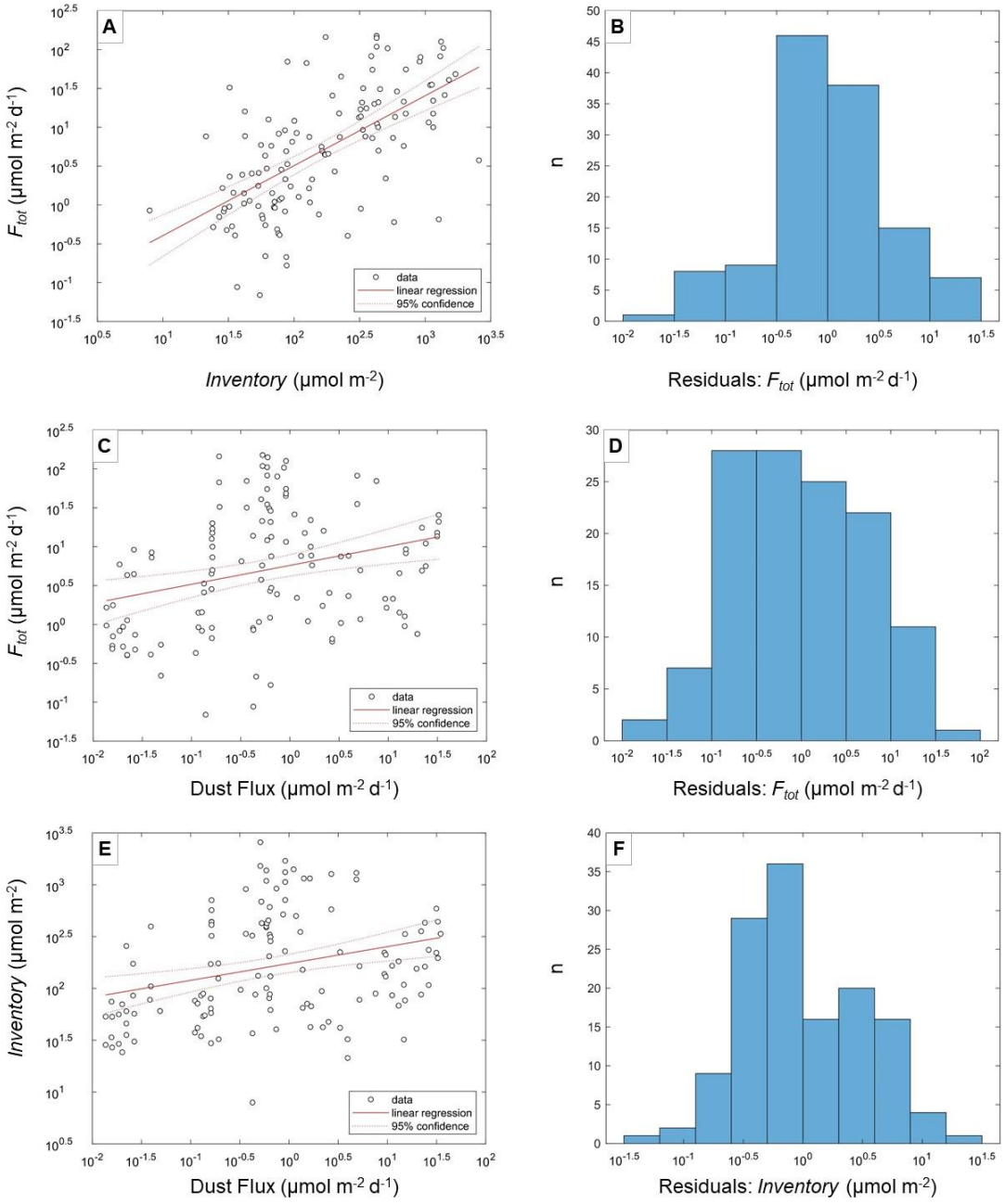

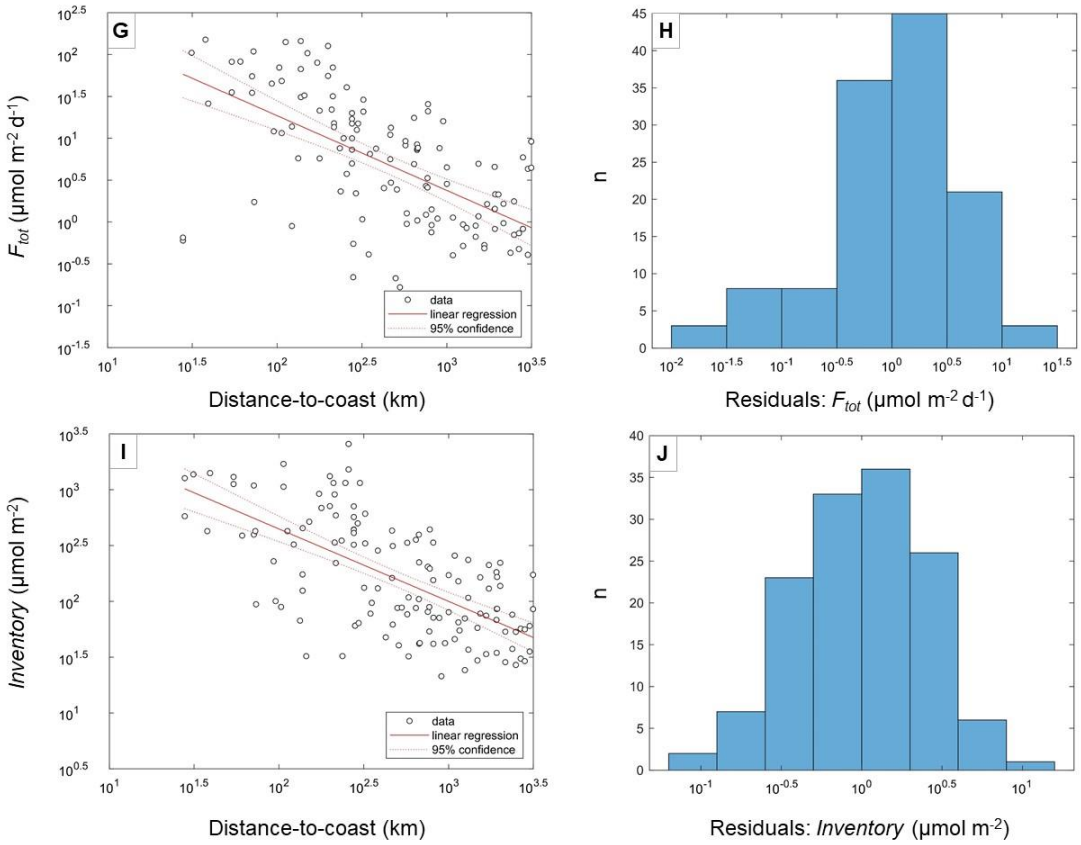
G
H
I
J
F_{tot} (µmol m^{-2} d^{-1})
Distance-to-coast (km)
Residuals: F_{tot} (µmol m^{-2} d^{-1})
Inventory (µmol m^{-2})
Residuals: *Inventory* (µmol m^{-2})
n
data
linear regression
95% confidence

Figure S3. Fe export is related to source proximity and the biological packaging of Fe. (A) Both F_{tot} and F_{POC}, an indicator of the local biological packaging potential or propensity for the formation of exportable material, decrease with increasing distance to coast. (B) F_{POC} is linked to F_{tot} (r^2 = 0.40, p < 0.005). (C) This is especially true in the High Latitude North Atlantic and Subantarctic (r^2 = 0.57, p < 0.005). Study sites in Panels B and C are color-coded by zone (See Figure 1).

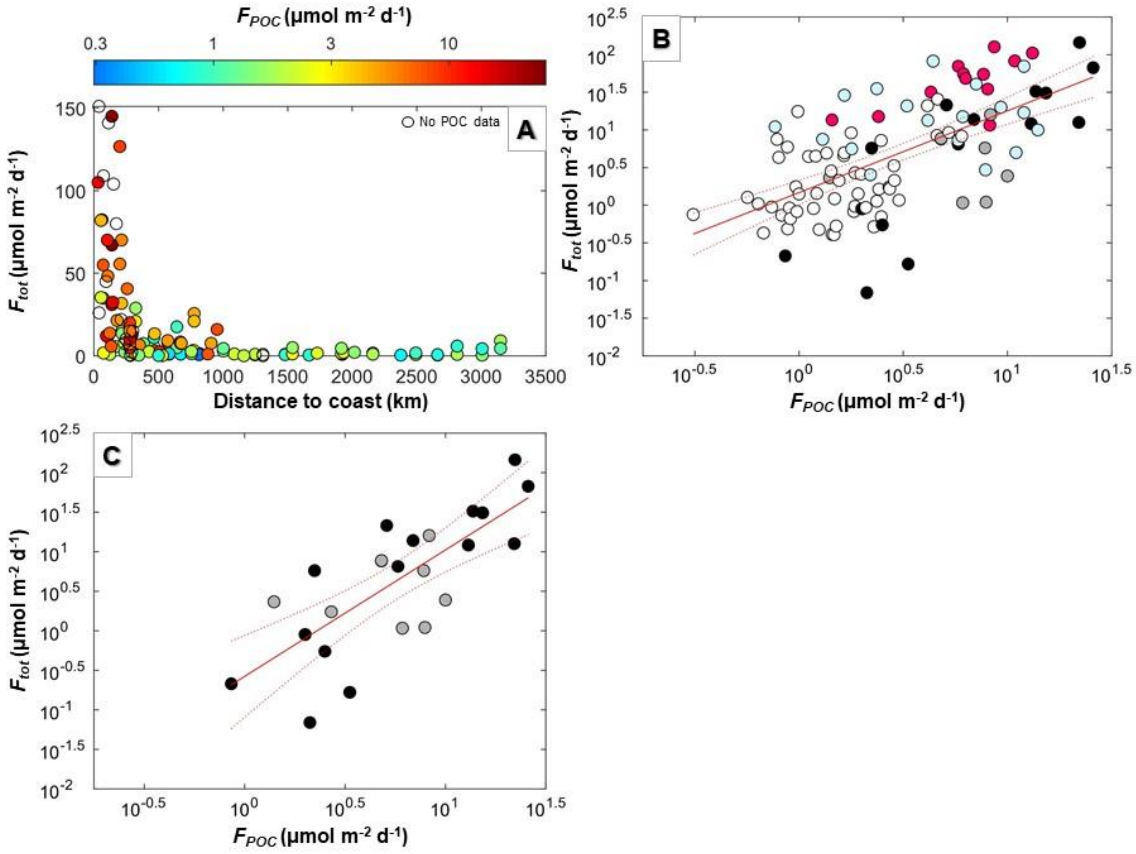

Figure S4. All τ_{tot} results by location and method. (Left) All residence time data are grouped by zone (See Figures 1 and 2). Locations that were removed from consideration in the main text are indicated in the dashed circles and labeled with the rationale for exclusion. Anomalies can occur as a result of methodological differences and atypical local conditions. The late stage eddy location is from off the coast of Peru from this study where an eddy was identified and almost 100% remineralization of POC was observed at 200 m. This remineralization produced an anomalously long τ_{tot} because the F_{tot} was so small compared to the high inventory. The under-collecting trap is from the Benguela Upwelling region (Noble et al., 2012). An anomalous particulate Fe measurement was found at the depth of export from this study in the North Atlantic. Lastly, the Gotland Basin is the only location where a moored trap was used (which can have different hydrodynamic issues) and the only semi-enclosed basin (Pohl et al., 2004). (Right) Methods are differentiated to assess whether either has a relative bias. The general overlap of data from these two methods is expected since sediment traps and ^{234}Th capture similar timescales when traps are deployed on the order of weeks to months. It has been suggested that sediment traps under-collect during periods of low (carbon) flux (Buesseler et al., 1994) and this would explain the slight offset between the sediment trap and the ^{234}Th-based results in the bottom third of this panel. Interestingly, sediment traps are also thought to over-collected in periods of high flux (Buesseler et al., 1994), but this is not observed here. Iron solubilization, in addition to hydrodynamic issues, could cause and underestimation of the actual sinking Fe flux, but comprehensive studies comparing simultaneous ^{234}Th-based and trap-based estimates would be needed to resolve this.

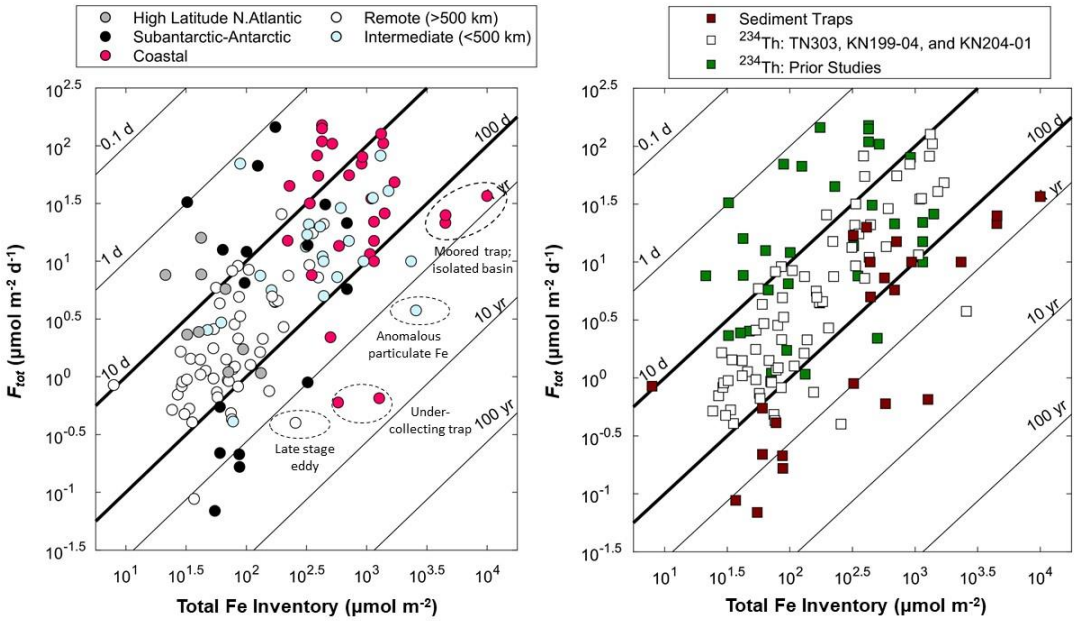

Figure S5. North Atlantic and South Pacific parameter comparisons for the determination of the residence time of lithogenic Fe. At most locations, aluminum data are not available for both particulate phases (large and small particles) that would be required to determine the full particulate lithogenic inventory of iron. Generally, only the large particle iron inventory of iron is calculable. We assume that the entire particulate inventory of iron is lithogenic to get a maximum τ_{lith} (x-axis) and this maximum estimate in used the main text for all stations. At stations where aluminum data for all particulate phases are available, we determine the 'actual' τ_{lith} (full particulate lithogenic inventory divided by F_{lith}, y-axis). A 1:1 line is shown in orange to indicate where the x and y parameters are equal. The linear regression for the data is shown in blue with its corresponding equation and coefficient of correlation. The regression suggests that, on average, the actual τ_{lith} is ~50% shorter than the maximum τ_{lith}.

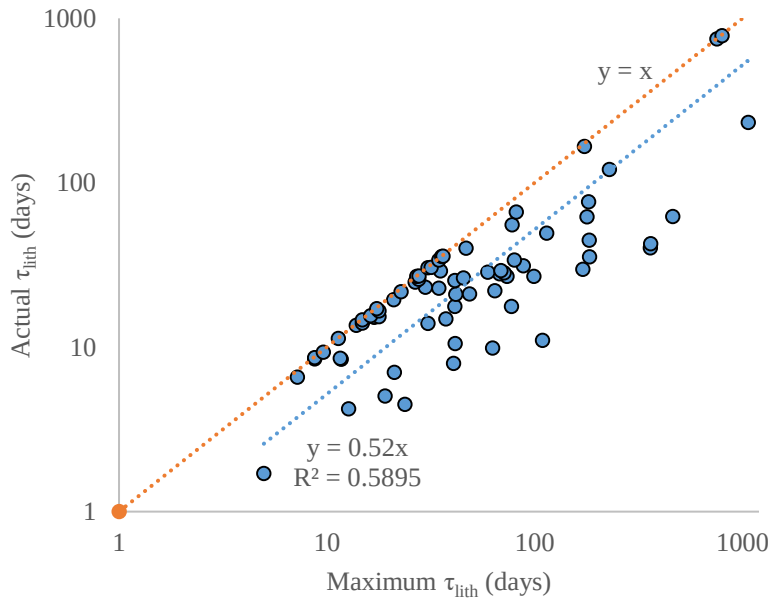

TABLES

Table S1. Study information and results related to iron export (flux) measurements. (included in separate file 'Blacketal_TablesS1_S2.xlsx)

Table S2. Study information and results related to iron residence time estimates. (included in separate file 'Blacketal_TablesS1_S2.xlsx)

Table S3. Statistical results from linear regression and multiple linear regression analyses of potential factors influencing Fe inventories, export fluxes (F_{tot}), and total residence times (τ_{tot}). Linear regressions are performed with x_1 as the independent variable and y as the dependent variable. Multiple linear regressions are performed with an additional independent variable, x_2. P-values less than 0.005 indicate significance. When the coefficient of determination (r^2) is > 0.20 the value is bolded.

x_1	x_2	y	r^2 (log-log)	p value
Total Fe inventory		F_{tot}	**0.48**	1E-18
Diss Fe Inventory		F_{tot}	**0.31**	7E-11
Dust flux		F_{tot}	0.09	1E-03
Dust flux		Total Fe inventory	0.09	5E-04
Dust flux		Diss Fe Inventory	**0.23**	2E-08
Distance to coast		F_{tot}	**0.46**	2E-17
Distance to coast		Total Fe inventory	**0.40**	4E-16
Distance to coast		Diss Fe Inventory	0.15	9E-06
Annual chl-a		F_{tot}	**0.42**	2E-15
Annual chl-a		Total Fe inventory	**0.33**	9E-13
Annual chl-a		Diss Fe Inventory	0.16	4E-06
16-day prior NPP		F_{tot}	0.01	4E-01
16-day prior NPP		Total Fe inventory	0.005	5E-01
16-day prior NPP		Diss Fe Inventory	0.03	8E-02
POC Flux		F_{tot}	**0.40**	7E-13
POC Flux		Total Fe inventory	0.14	1E-04
POC Flux		Diss Fe Inventory	0.05	3E-02

Table continued on next page

Table S3 continued.

x_1	x_2	y	r^2 (log-log)	p value
Dust flux		τ_{tot}	0.02	0.2
Dust flux		τ_{diss} (τ_{bio})	0.16	5E-05
Dust flux		τ_{diss} ($\tau_{bio+auth}$)	0.20	4E-06
Distance to coast		τ_{tot}	0.12	1E-04
Distance to coast		τ_{diss} (τ_{bio})	0.0003	0.9
Distance to coast		τ_{diss} ($\tau_{bio+auth}$)	0.01	0.4
Annual chl-a		τ_{tot}	0.14	6E-05
Annual chl-a		τ_{diss} (τ_{bio})	0.03	0.1
Annual chl-a		τ_{diss} ($\tau_{bio+auth}$)	0.04	0.06
16-day prior NPP		τ_{tot}	0.003	0.6
16-day prior NPP		τ_{diss} (τ_{bio})	0.012	0.3
16-day prior NPP		τ_{diss} ($\tau_{bio+auth}$)	0.001	0.8
F_{POC}		τ_{tot}	**0.30**	2E-09
F_{POC}		τ_{diss} (τ_{bio})	0.09	3E-03
F_{POC}		τ_{diss} ($\tau_{bio+auth}$)	0.10	1E-03
Distance to coast	F_{POC}	Total Fe inventory	**0.43**	6E-15
Distance to coast	Annual chl-a	Total Fe inventory	**0.42**	1E-14
Distance to coast	F_{POC}	Diss Fe Inventory	**0.31**	2E-09
Distance to coast	Annual chl-a	Diss Fe Inventory	**0.26**	1E-07
Distance to coast	F_{POC}	F_{tot}	**0.52**	4E-18
Distance to coast	Annual chl-a	F_{tot}	**0.48**	2E-16
Distance to coast	F_{POC}	τ_{tot}	0.16	2E-04
Distance to coast	Annual chl-a	τ_{tot}	0.14	8E-04
Distance to coast	F_{POC}	τ_{diss} (τ_{bio})	0.06	0.1
Distance to coast	Annual chl-a	τ_{diss} (τ_{bio})	0.10	0.02
Distance to coast	F_{POC}	τ_{diss} ($\tau_{bio+auth}$)	0.01	0.8
Distance to coast	Annual chl-a	τ_{diss} ($\tau_{bio+auth}$)	0.06	0.1

Table S4. ^{234}Th flux results. Fluxes are reported in decays per minute per square meter per day at 100 m and 200 m. [a] Uncertainty > flux estimate. [b] Calculated flux is negative. [c] 200 m is > bottom depth.

Cruise	Station	Latitude (North)	Longitude (East)	^{234}Th flux 100 m (dpm m^{-2} d^{-1})	^{234}Th flux 200 m (dpm m^{-2} d^{-1})
TN303	15	-16.0	-104.0	1965 ± 96	2078 ± 172
TN303	17	-15.0	-109.2	1427 ± 116	1132 ± 180
TN303	18	-15.0	-112.8	1587 ± 101	1392 ± 191
TN303	21	-14.8	-115.0	1386 ± 117	1201 ± 184
TN303	23	-14.0	-120.0	1845 ± 108	1667 ± 211
TN303	25	-12.5	-125.0	1477 ± 98	1474 ± 256
TN303	26	-11.7	-128.0	1447 ± 102	926 ± 200
TN303	28	-11.6	-132.5	1483 ± 114	1363 ± 224
TN303	30	-11.6	-137.0	1417 ± 106	1307 ± 191
TN303	32	-11.0	-142.9	1756 ± 110	1854 ± 187
TN303	34	-10.8	-147.5	1608 ± 110	1592 ± 195
TN303	36	-10.5	-152.0	1122 ± 104	1096 ± 248
TN303	7	-12.0	-84.0	2801 ± 402	2080 ± 438
TN303	9	-12.0	-89.0	1407 ± 104	301 ± 203
TN303	11	-12.0	-94.0	1886 ± 91	1686 ± 149
TN303	13	-14.0	-99.0	1295 ± 108	944 ± 217
TN303	2	-12.0	-77.4	7334 ± 693	--[c]
TN303	3	-12.0	-77.7	6918 ± 1206	--[c]
TN303	4	-12.0	-77.8	6088 ± 938	5877 ± 964
TN303	5	-12.0	-78.2	6079 ± 753	5157 ± 699
TN303	1	-12.0	-79.2	6053 ± 938	5956 ± 950
KN204-01	6	37.6	-68.4	809 ± 87	1165 ± 146
KN204-01	4	38.3	-68.9	170 ± 92	--[b]
KN204-01	3	38.8	-69.2	779 ± 91	582 ± 139
KN204-01	2	39.4	-69.5	1714 ± 81	1920 ± 139
KN204-01	1	39.7	-69.8	1215 ± 104	1947 ± 160
KN204-01	22	19.4	-29.4	67[a] ± 124	--[b]
KN204-01	20	22.3	-35.9	263 ± 103	436 ± 161
KN204-01	18	24.2	-40.2	261 ± 106	145[a] ± 159
KN204-01	16	26.1	-44.8	178 ± 122	39[a] ± 172
KN204-01	14	27.6	-49.6	269 ± 96	12 [a] ± 157
KN204-01	12	29.7	-56.8	520 ± 103	414 ± 146
KN204-01	10	31.9	-64.1	64[a] ± 101	--[b]
KN204-01	8	35.4	-66.5	275 ± 95	405 ± 152

Table continued on next page

Table S4 continued.

Cruise	Station	Latitude (North)	Longitude (East)	^{234}Th flux 100 m (dpm m^{-2} d^{-1})	^{234}Th flux 200 m (dpm m^{-2} d^{-1})
KN199-04	9	17.4	-18.3	1148 ± 95	918 ± 150
KN199-04	10	17.4	-20.8	814 ± 98	484 ± 156
KN199-04	11	17.4	-22.8	741 ± 90	648 ± 145
KN199-04	12	17.4	-24.5	153 ± 84	13[a] ± 167
KN204-01	24	17.4	-24.1	963 ± 136	1415 ± 216
KN199-04	1	38.3	-9.7	929 ± 105	1369 ± 168
KN199-04	3	35.2	-16.0	303 ± 99	578 ± 188
KN199-04	5	31.0	-22.0	404 ± 129	332 ± 199
KN199-04	7	24.0	-22.0	629 ± 92	844 ± 177

Table S5. Testing different approaches for the use of below detection limit results from the Pacific (cruise TN303) with iron export flux calculations. Grey shading indicates stations where a difference in the flux between cases was observed. Groups P1 (Gyre), P2 (Offshore), and P3 (Coastal-Shelf) correspond to those described in Ohnemus et al., 2016. Zonal averages (± 1 s.d.) indicate that changing the method of use of the BDL results does not significantly impact flux calculations. LP indicates large particle Fe concentrations collected using >51 μm filters.

		Fe flux at 100 m (μmol m^{-2} d^{-1})		
Group	**TN303 station**	**Case 1:** Use all BDL $[Fe]_{LP}$ as measured	**Case 2:** All BDL $[Fe]_{LP}$ set to detection limit	**Case 3:** All BDL $[Fe]_{LP}$ removed before calculations
P3	1	56	56	56
	2	105	105	105
	3	82	82	82
	4	55	55	55
	5	12	12	12
P2	7	8	8	8
	9	1.0	1.1	1.4
	11	0.5	0.5	0.5
	13	0.5	0.5	No result
P1	15	1.6	1.7	2.0
	17	0.3	0.7	No result
	18	0.8	0.8	0.8
	21	0.4	0.4	No result
	23	9	9	9
	25	0.5	0.5	0.5
	26	2.8	2.9	No result
	28	1.4	1.4	1.4
	30	0.9	0.9	1.0
	32	2.9	2.9	2.9
	34	2.6	2.6	2.6
	36	1.4	1.4	1.4
Average ± s.d.				
P1 (15 to 36)		2.0 ± 2.4	2.1 ± 2.4	2.4 ± 2.6
P2 (7 to 13)		0.9 ± 0.5	1.0 ± 0.5	1.3 ± 0.7
P3 (1 to 5)		62 ± 35	62 ± 35	62 ± 35

Table S6. Testing different approaches for the use of below detection limit results from the Pacific (cruise TN303) with iron inventory calculations. Grey shading indicates stations where a difference in the flux between cases was observed. Groups P1 (Gyre), P2 (Offshore), and P3 (Coastal-Shelf) correspond to those described in Ohnemus et al., 2016. Cases are the same as indicated in Table S5. Total inventory includes large particle, small particle, and dissolved concentrations, which incorporates BDL changes to both the large particle and small particle datasets. Inventory results for each case at individual stations and zonal averages (± 1 s.d.) indicate that changing the method of use of the BDL results can significantly impact the total inventory.

		Large particle Fe inventory 100 m ($\mu mol\ m^{-2}$)			**Total Fe inventory 100 m ($\mu mol\ m^{-2}$)**		
Group	**TN303 station**	**Case 1**	**Case 2**	**Case 3**	**Case 1**	**Case 2**	**Case 3**
	1	369	369	369	670	670	670
	2	249	249	249	707	707	707
P3	3	83	83	83	187	187	187
	4	98	98	98	294	294	294
	5	624	624	624	973	973	973
	7	49	49	49	87	91	98
	9	4	4	8	24	29	134
P2	11	3	3	3	7	17	50
	13	2	3	5	19	26	40
	15	7	8	10	12	22	No result
	17	1	2	11	4	17	23
	18	2	3	4	9	16	13
	21	2	2	3	25	26	12
	23	14	15	26	70	73	37
	25	4	4	4	11	19	17
P1	26	3	5	26	6	19	No result
	28	6	6	6	14	22	55
	30	5	6	12	13	21	29
	32	51	51	51	58	63	16
	34	19	19	19	42	44	53
	36	17	18	23	31	33	38
Average ± s.d.							
P1 (15 to 36)		11 ± 14	12 ± 14	16 ± 14	25 ± 22	31 ± 19	29 ±16
P2 (7 to 13)		4 ± 2	4 ± 2	7 ± 3	15 ± 7	24 ± 5	75 ± 51
P3 (1 to 5)		285 ± 223	285 ± 223	285 ± 223	566 ± 322	566 ± 322	566 ± 322